BMC Medical Genomics

RESEARCH

Open Access

Bioinformatics identification and validation of pyroptosis-related gene for ischemic stroke

Xinying Shang[1†], Rui Wei[1†], Di Yang[1], Bawei Yu[1] and Wei Zhang[1*]

Abstract

Background Ischemic stroke (IS) is one of the common and frequent diseases with extremely high lethality and disability in the world, and there is no effective treatment at present. This study aimed to screen hub genes involved in cerebral ischemia/reperfusion injury (CIRI) and pyroptosis, and explore promising intervention targets.

Methods CIRI-related genes (GSE202659 and GSE131193) and pyroptosis-related genes (PRGs) in mice were obtained from the Gene Expression Omnibus (GEO) and GeneCards database. We screened for LASSO regression to construct a prognostic model of GSE131193 and PRGs and examined by GSE137482. The functional enrichment analysis of Gene Ontology (GO), Kyoto Encyclopedia of Genes and Genomes (KEGG), Gene Set Enrichment Analysis (GSEA) and Gene Set Variation Analysis (GSVA) were performed on pyroptosis-related differentially expressed genes (PRDEGs) of GSE202659.The key modules for CIRI and pyroptosis were identified by Weight Gene Co-expression Network Analysis (WGCNA). Subsequently, Protein-protein Interaction (PPI) network and the Cytoscape was constructed to screen out hub genes. Used the starBase to predict miRNA interacting with hub genes and constructed mRNA-miRNA-lncRNA interaction networks. CIRI-related Molecular Subtypes were constructed for hub genes. The relationship between immune cells and hub genes was verified via CIBERSORT. Finally, we selected C57BL/6 mice to construct models to confirm hub genes by enzyme linked immunosorbent assay (ELISA), reverse transcription-polymerase chain reaction (RT-PCR), western blot, and Immunofluorescence.

Results A total of 272 PRGs and 35 PRDEGs were screened. An eight-gene risk prediction models were established (AUC = 0.868). GO, KEGG, GSEA and GSVA analyses revealed that PRDEGs were mainly involved in positive regulation of cytokine production, and NOD-like receptor signaling pathway. And then, seven hub genes (*Irf1*, *Icam1*, *Tlr2*, *Tnf*, *Cebpb*, *Il1rn*, and *Casp8*) were identified by PPI. *Icam1*, *Tnf*, *Cebpb*, *Il1rn*, and *Casp8* had high expression profiles in Cluster2 by hierarchical clustering. The immune infiltration analysis results showed that among the hub genes, *Cebpb*, *Il1rn*, and *Casp8*, showed a significant positive correlation with the degree of NK.Actived, and *Icam1* showed a significant negative correlation with B.Cells.Memory. The results of animal experiments significantly demonstrated an upregulation of *Irf1*, *Icam1*, *Tlr2*, *Cebpb*, and *Il1rn*.

†Xinying Shang and Rui Wei contributed equally to this work and share first authorship.

*Correspondence:
Wei Zhang
zhangwei7222@kmmu.edu.cn

Full list of author information is available at the end of the article

Conclusion Our finding indicated that *Irf1*, *Icam1*, *Tlr2*, *Cebpb*, and *Il1rn* are hub genes associated with pyroptosis, and these genes are all associated with different immune cells, so as to provide new targets for the prevention and treatment of IS from the perspective of pyroptosis.

Keywords Pyroptosis, Cerebral ischemia reperfusion injury, Ischemic stroke, IRF1, Immune cell infiltration

Introduction

Cerebral stroke is a general term for localized cerebral blood circulation disorders that cause neurological dysfunction. The Lancet Neurology [1] states that in 2019, an estimated 12.2 million new cases of stroke occurred, with a total of 101 million cases globally. Stroke can be classified into two types: ischemic and hemorrhagic, with ischemic stroke (IS) accounting for more than 70% of all strokes [2]. IS are mainly caused by the occlusion of the cerebral arteries, resulting in local or large-scale hypoxia and ischemia of the patient's brain tissue, which leads to apoptosis of neuronal cells and tissue necrosis. Early restoration of blood perfusion to the ischemic area [3, 4] (e.g., pharmacological thrombolysis or mechanical thrombolysis) is the main clinical treatment for IS; however, after acute revascularization, reperfusion injury that occurs at the site of ischemia forms a secondary blow to the brain tissues, namely, cerebral ischemia reperfusion injury (CIRI). Despite significant advances in IS therapeutic strategies, most patients have unsatisfactory outcomes, which may be because of a lack of a clear understanding of pathological processes involved in its development.

Pyroptosis called one of programmed cell death formally proposed by Cookson et al. in 2001 [5], which relies on the activation of the cleavage of inflammatory cysteine asparaginases and causes the release of multiple pro-inflammatory substances. The main manifestations [6] are osmotic swelling of cells, rapid rupture of membranes, and the release of cytoplasmic contents. Pyroptosis [7] can be widely involved in the occurrence and development of IS, accompanied by inflammasome activation (e.g., NOD-like receptor thermal protein domain associated protein 3 (NLRP3), etc.) and upregulation of interleukin-1β (IL-1β) and interleukin-18 (IL-18) levels, so as to trigger a post-ischemic inflammatory response that exacerbates brain tissue damage. Therefore, we speculate that targeting key genes in the pyroptosis pathway may reduce parenchymal injury, decrease the level of inflammation, and ameliorate neurological damage caused after IS. Stimulator of Interferon Genes (STING) is an endoplasmic reticulum membrane protein that has recently been described as an important intrinsic immune bridging protein related to neuroinflammation. Li et al. [8] found that STING can regulate NLRP3 mediated microglial pyroptosis after MCAO and so then reduce neuroinflammation caused by CIRI. And Caspase-1 inhibitors can inhibit the expression of gasdermin D (GSDMD), inflammatory vesicles, caspase-1, and IL-1β by targeting typical focal inflammatory response pathways thereby exerting a protective effect on the membrane structure of neurons after cerebral ischemic injury [9]. The above findings suggest that pyroptosis is a potential target for intervention in ischemic stroke. Although we have gained some understanding of pyroptosis in stroke, stroke remains the third leading cause of death globally due to the absence of effective treatment [10]. We aimed to seek new genes involved in CIRI and pyroptosis so as to providing new treatments for IS.

Bioinformatics offers new tools for identifying potential biomarkers, and exploring disease mechanisms, and so on. For example, Liu [11] found that there was a causal relationship between blood pressure, certain circulating lipids, and the development of IS by Bioinformatics, which has some guidance for clinical diagnosis and treatment. Therefore, the identification and study of differentially expressed pyroptosis-related genes (PRGs) in IS can help recognize the role of pyroptosis in the development and regression of IS, and may provide new ideas for the clinical treatment of IS. In this study, we proposed to mine the Gene Expression Omnibus (GEO) database and GeneCards database to screen hub genes affecting CIRI associated with pyroptosis and validate hub genes by animal experiments. Our findings will provide novel ideas for further searching for promising intervention targets of IS.

Material methods

Datasets and quality control

The GEOquery [12] (Version 2.56.0) package of R software (Version 4.0.0, http://r-project.org/) was used to download from the GEO (https://www.ncbi.nlm.nih.gov/geo/) database [13] reliable sources of samples for mouse CIRI-related expression profiling datasets GSE131193 [14] (GPL19057 Illumina NextSeq 500) and GSE202659 [15] (GPL24247 Illumina NovaSeq 6000), while mouse cerebral ischemia injury-related dataset GSE137482 [16] (GPL19057 Illumina NextSeq 500) was manually retrieved for model validation. The samples in these three datasets were all from Mus musculus. 27 control samples and 27 cerebral ischemia-injury samples from these three datasets were included in this study. The raw data of these three datasets were read using the affy package (Version 1.66.0) to obtain the gene expression matrices of these two datasets. The GeneCards (https://www.genecards.org/) database [17] was searched using pyroptosis

as the keyword, and human-derived PRGs were identified. Subsequently, homologous gene conversion between mice and humans was performed using the R package biomaRt (Version 2.46.3) to obtain mouse-derived PRGs.

Differential molecular screening

The expression profiles of PRGs in the CIRI subgroups were screened in GSE202659 for correlation analysis, and gene expression correlations were visualized using R packages corrplot (Version 0.92) and RColorBrewer (Version 1.1-3) to explore the co-expression of PRGs.

GSE202659 was analyzed for differential expression using DESeq2 package (Version 1.28.1), and genes satisfying adj. p-value < 0.05 and|log2FC| ≥ log21.5 were identified as differentially expressed genes (DEGs), specifically categorized as pyroptosis-related differentially expressed genes (PRDEGs). Volcano plots of PRDEGs were drawn using the ggplot2 package (Version 3.3.5), ggrepel package (Version 0.9.2), and cowplot package (Version 1.1.1); heatmaps of PRDEGs were drawn using the pheatmap package (Version 1.0.12) and gplots package (Version 3.1.3) to demonstrate the differential expression of PRDEGs; and boxplots were drawn using the ggpubr package (Version 0.5.0) to further demonstrate the differential expression of PRDEGs between control and CIRI groups.

One-way logistic regression analysis and LASSO regression to construct models

The expression profiles of PRGs were screened in GSE131193 for one-factor logistic regression analysis. Risk and protective factors were initially identified in the PRGs in the CIRI-grouped samples, and least absolute shrinkage and selection operator (LASSO) regression was commonly used to construct prognostic models. We used the R package glmnet (Version 4.1-6) for LASSO regression based on one-way logistic regression analysis to further screen the influencing factors and construct the model. GSE137482 was used as the validation dataset to test the predictive performance of the model, and the R packages ROCR (Version 1.0–11) and ggpubr (Version 0.5.0) were used to calculate the ROC values as well as to show the differences in the risk scores of the samples in GSE137482.

Functional enrichment analysis

Gene Ontology (GO) and Kyoto Encyclopedia of Genes and Genomes (KEGG) enrichment analyses were performed on the PRDEGs using the clusterProfiler package (Version 3.16.1), respectively, after ID conversion of mouse genes using the R package org.Mm.eg.db (Version 3.12.0) Pathway maps of KEGG enrichment results were downloaded via the R package pathview (Version 1.28.1), and *adj. p-values* < 0.05 were considered statistically different. Gene Set Enrichment Analysis (GSEA) was also performed on the gene expression matrices through the clusterProfiler package (Version 3.16.1) and "m2.cp.v2022.1. Mm.symbols.gmt" as the reference gene set, false discovery rate (FDR) < 0.25 with $p < 0.05$ was considered significantly enriched. Specific gene sets from the KEGG database were selected using the R package msigdbr (Version 7.5.1), and the expression profiles were subjected to Gene Set Variation Analysis (GSVA) using the GSVA package (Version 1.36.3) and limma package [18], which satisfied *adj. p-value < 0.05* and|log2FC|>1 filtering for the differential pathway.

Screening and correlation analysis of hub genes

We performed WGCNA (Version 1.70-3) analysis on GSE131193, constructed a PRG-based co-expression network, obtained modules and genes associated with the CIRI phenotype. We also used the VennDiagram package (Version 1.7.3) to show the intersecting genes between the related module genes and PRDEGs and used the STRING database to construct protein-protein Interaction (PPI) networks for the intersecting genes. Cytoscape [19] was used to visualize the PPI network, the topological properties of the nodes and edges in the network were analyzed using the Network Analyzer [20] tool, and the subnetworks were filtered using MCODE [21]. We then searched for mouse miRNA interaction data with target genes using the starBase database (Version 2.0, https://starbase.sysu.edu.cn/) [22] to obtain miRNA-mRNA and miRNA-lncRNA regulatory relationship pairs. The intersecting genes between related module genes and PRDEGs were mapped to the interworking data to extract the mRNA-miRNA-lncRNA ternary regulatory relationships, and the network was topologically analyzed and visualized using Cytoscape. Expression profiles of PRDEGs in samples that experienced stroke were extracted from GSE131193 for CIRI-related molecular isoform construction and analysis. The R package pheatmap (Version 1.0.12) was used for expression differences. The R package ggpubr (Version 0.5.0) was used to demonstrate correlations.

Immune cell infiltration correlation analysis

We obtained a mouse immune cell signature gene set from the literature [23], uploaded the gene expression matrix data from GSE131193 to CIBERSORT, and filtered the output of samples that were not expressed in half of the samples to derive the immune cell infiltration matrix. Heatmaps were plotted using the R language pheatmap package (Version 1.0.12), and calculated the correlations between immune cell infiltration and hub genes. Then the results of the correlation analysis are presented using the R package linkET (Version 0.0.7.1) [24].

Middle cerebral artery occlusion (MCAO) construction and neurobehavioral scoring

SPF-grade C57BL/6 male mice (6–8 weeks) were purchased by Kunming Medical University, weighing 20–25 g. All experiments have been approved by Kunming Medical University (No. kmmu20221789). Four mice were used in each group. The mice were anesthetized using isoflurane (RWD, R510-22-10), and the right middle cerebral artery was blocked by inserting a Guangzhou Jialing wire tether (L1800). The wire tether was removed 2 h after the ischemia. In the sham group, only the ICA was ligated without blocking the middle cerebral artery.

We scored the neurological deficits in all C57BL/6 mice participating in the experiment according to the Bederson method [25]. The specific criteria were as follows: score 0 indicated that the mice had normal neurological function without ischemia; score 1 indicated that the mice underwent inward flexion to the left forelimb; score 2 indicated that the mice walked in the left direction; and score 3 indicated that the mice circled to the left in a tail-chasing-like manner. If the score was higher than one, the mice continued to participate in subsequent experiments. Mice that died or scored 0 after MCAO modeling were excluded, and the number of mice required for this experiment was determined using the difference-in-difference method.

Table 1 Primer sequences for RT-PCR

Gene	Sequences (5′-3′)
GAPDH	F: CCTCGTCCCGTAGACAAAATG; R: TGAGGTCAATGAAGGGGTCGT
Irf1	F: ACCCTGGCTAGAGATGCAGATTA; R: TTGTTGATGTCCCAGCCGT
Icam1	F: GTACTGTACCACTCTCAAAATA-ACTGG; R: TGGGGCTTGTCCCTTGAGT
Tlr2	F: CCAAAGTCTAAAGTCGATCCGC; R: AGCCCATTGAGGGTACAGTCGT
TNF	F: CCCTCACACTCACAAACCACC; R: CTTTGAGATCCATGCCGTTG
Cebpb	F: TGGACAAGCTGAGCGACGAG; R: TTGAACAAGTTCCGCAGGGT
Il1rn	F: CTCTCCTTCTCATCCTTCTGTTTCA; R: TCCTTGTAAGTACCCAGCAATGAG
casp8	F: CTTGAAGGAAGGGAAGAGTTGC; R: CACTGTCTTGTTCTCTTGGCGA
Caspase-1	F: GGCTGACAAGATCCTGAGGG; R: TAGGTCCCGTGCCTTGTCC
IL-1β	F: GTAATGAAAGACGGCACACCC; R: CAGGCTTGTGCTCTGCTTGTG
IL-18	F: CCATGTCAGAAGACTCTTGCGT; R: CAAAGTTGTCTGATTCCAGGTCTC
NLRP3	F: ATGACTTTCCAGGAGTTCTTCGC; R: CCAAAGAGGAATCGGACAACAA
GSDMD	F: AGTGCTCCAGAACCAGAACCG; R: TCACCACAAACAGGTCATCCC
ASC	F: CTATCTGGAGTCGTATGGCTTGG; R: CAAAGTGTCCTGTTCTGGCTGT

TTC staining

The whole brains of the mice were immediately removed after modeling and transferred to the refrigerator at -20 °C for freezing for 15 min, and they were sectioned into 6 coronal slices. The slices were placed into 5 ml of 2% TTC staining solution (Sigma, T8877-10G) for 30 min at 37 °C. And then, take Photographs after 24 h of immobilization, and the data was analyzed by using ImageJ software. We used this formula to calculate: relative infarct area (%) = infarct area/total brain area ×100%.

HE staining

The brain tissue was buffer-fixed with 0.9% saline and 4% paraformaldehyde and embedded in paraffin. The thickness of every paraffin section was approximately 5 μm. And then, using hematoxylin and eosin staining kit (Beyotime, C0105S) and photographed under a microscope for histopathological analysis.

Nissl staining

The 5 μm paraffin sections of the brain were dewaxed and rehydrated, stained with Nissl Staining Solution (Beyotime, C0117), and subsequently photographed and analyzed under a microscope.

Reverse transcription-polymerase chain reaction (RT-PCR)

After MCAO, a portion of fresh brain tissue was transferred to enzyme-free EP tubes, TRIZOL reagent (Invitrogen, 15596026) was added to the tubes, and the tissue samples were crushed thoroughly cDNA was extracted (Thermo Fisher, K1622), amplified via PCR (Roche, 4913914001), and analyzed using the $2^{-\rho\rho Ct}$ method. *GAPDH* is an internal reference in each group in four independent experiments. The sequences of primers were shown as Table 1.

Enzyme linked immunosorbent assay (ELISA)

We collected mouse serum and detected the levels of *IL-1β* (Beyotime, PI301) and *IL-18* (Beyotime, PI553) separately by using ELISA kits.

Western blot

BCA method was used, protein uploading, gel electrophoresis, membrane transfer, 5% milk powder blocked for 2 h, plus primary antibody (*NLRP3* (Proteintech, 68102-1-Ig), *Caspase-1* (Cell Signaling Technology, 83383), *GSDMD* (Affinity, AF4012), *Irf1* (Cell Signaling Technology, 8478), and *α-Tubulin* (Abcam, ab7291) were incubated overnight (at least 12 h) at 4 °C, and the secondary antibodies (Proteintech, SA00001-2, SA00001-1) were incubated for 2 h. The development solution was

added dropwise in a chemiluminescence imager (GE, Amersham Imager 600) to develop and take pictures for semi-quantitative analysis of the grayscale of the target protein bands and the α-Tubulin protein bands using Image J software.

Immunofluorescence

Brain sections were deparaffinized for antigen repair, followed by 10% goat serum (Solarbio, SL038) incubation for 2 h, addition of primary antibodies *Irf1* (Cell Signaling Technology, 8478) and *NeuN* (Cell Signaling Technology, 94403) incubated at 4 ℃ overnight, addition of fluorescent secondary antibodies (Proteintech, SA00013-2, SA00001 -1), incubated at room temperature and protected from light for 2 h, and sealed with DAPI sealer (Sigma-Aldrich, F6057). Fluorescence microscope (Olympus, BX53) was used for observation and image acquisition.

Statistical description

All bioinformatic data calculations and statistical analyses were performed using R software (Version 4.0.0). For comparisons of continuous variables between the two groups, Student's t-tests were used to estimate the statistical significance of normally distributed variables. All animal experimental data were expressed as mean ± standard deviation (SD) using GraphPad Prism software (Version 9.5), in which comparisons between two groups were first tested for normal distribution and then t-tested. If not specifically specified, all statistical P-values are bilateral. When $p < 0.05$, all data were considered statistically significant.

Results

Variance analysis

Gene expression matrices of GSE202659 and GSE131193 were processed using the GEO data platform. After data preprocessing, we obtained expression profiles of 272 pyroptosis-related genes from GeneCards and utilized the STRING database to analyze their interaction network. The interactions were generated between 257 genes under the condition that the combined score was ≥ 0.4 (Fig. 1B). The PRGs of the GSE202659 data were analyzed for correlation using the R software, and the top 56 genes in the correlation ranking were mapped using a correlation heat map (Fig. 1C). The results showed that nearly 37% of the selected PRGs had a positive correlation of ≥ 0.6 between gene pairs, and more than 23% had a negative correlation of ≥-0.6 between gene pairs. Subsequent differential expression analysis of the gene expression matrix of the GSE202659 data extracted 31 upregulated genes and four downregulated genes (35 *corrplots*) compared to the normal samples, and the top eight genes with the most significant differences were annotated by volcano plots (Fig. 1E). The heatmap shows the PRDEGs in GSE202659 in the control and CIRI groups, respectively (Fig. 1D). Subsequently, intergroup expression analysis of PRDEGs was performed and filtered according to a p-value < 0.05, with 33 of the genes visualized in box plots (Fig. 1F).

Risk modeling based on PRDEGs

After one-way logistic analysis, 272 PRGs in GSE131193 were screened for 29 significant variable genes based on a p-value < 0.05, followed by 10-fold cross-validation and minimum criterion and feature selection using the LASSO regression model (Fig. 2A, $\lambda \approx 0.00126$), which finally identified Stxbp2, Vtn, Atg3, Prim1, Mettl14, Birc3, Ets1, and Prdm1 as modeled significant genes. The GSE137482 was used to validate the prognostic risk model by calculating the risk score, constructing the ROC curve (Fig. 2B), and obtaining an AUC of 0.868, which proved that the constructed model has good prediction performance on the external dataset with high robustness. Finally, the risk scores of the control and CIRI groups in GSE137482 were visualized in a box plot (Fig. 2C), which showed that the risk score was higher in the CIRI group than in the control group.

Enrichment analysis of PRDEGs

The 35 PRDEGs were analyzed by GO and KEGG (Supplementary Tables 1,2) enrichment analysis. The GO results showed that PRGs were mainly related to positive regulation of cytokine production, membrane rafts (Fig. 3A), while the KEGG results showed that PRGs were enriched in the NOD-like receptor signaling pathway, lipid and atherosclerosis (Fig. 3B). The two most significant pathways, the NOD-like receptor signaling pathway and lipid and atherosclerosis, were also mapped by KEGG database search, and the corrected p-value of the enrichment results of the two pathways was less than 0.01 (Fig. 3C, E). The GSEA enrichment of GSE202659 was performed by selecting "m2.cp.v2022.1.Mm.symbols.gmt" as the reference gene set, with FDR of < 0.25 and $p < 0.05$ as significantly enriched pathways (Supplementary Table 3). GSEA analysis showed that PRGs in GSE202659 were present in up-regulated pathways such as the tumor necrosis factor (TNF) signaling pathway ($p < 0.05$), rheumatoid arthritis ($p < 0.05$), and prion diseases ($p < 0.05$) and were significantly enriched in downregulated pathways (Fig. 3D). Furthermore, these PRGs were significantly enriched in the downregulated calcium signaling ($p < 0.01$) and Rap1 signaling pathways ($p < 0.05$) (Fig. 3F). Performing GSVA analysis (Supplementary Table 4) on pathways within GSE202659 showed that the differential pathways in GSE202659 were KEGG_PRION_DISEASES ($p < 0.01$), KEGG_SYSTEMIC_LUPUS_ERYTHEMATOSUS ($p < 0.01$), and

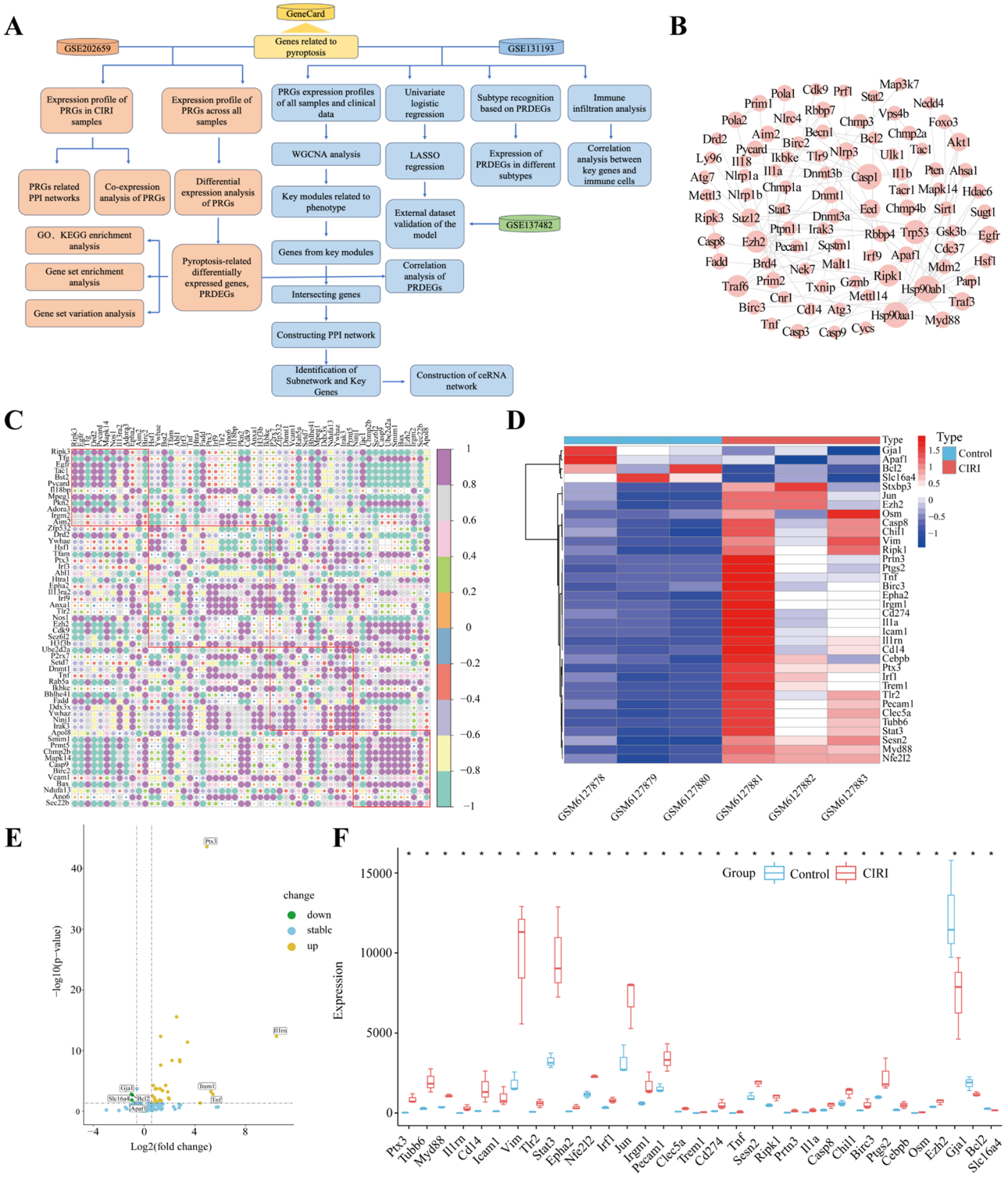

Fig. 1 Screening and risk model construction of PRDEGs. (**A**) Presentation of the technical route. (**B**) Interaction network diagram of PRGs. (**C**) Heatmap of PRGs correlation in GSE202659. (**D**) GSE202659 heatmap. (**E**) GSE202659 volcano plot. (**F**) Significant expression box plot of PRDEGs

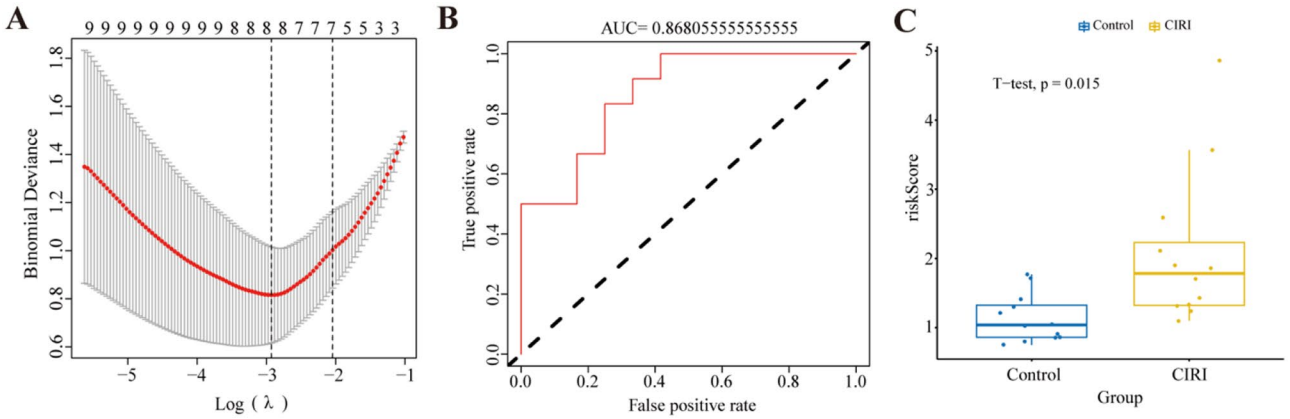

Fig. 2 Risk model construction and validation of PRDEGs based on GSE131193. (**A**) Feature selection by using the LASSO regression model. (**B**) ROC curves. (**C**) Boxplot of risk scores

KEGG_ECM_RECEPTOR_INTERACTION ($p < 0.05$) (Fig. 3G).

CIRI gene hub gene screening

Data preprocessing yielded a gene expression matrix for GSE131193, from which we extracted clinical information from 272 genes, 12 control samples, and 12 CIRI samples. We clustered the samples in GSE131193 using Pearson's correlation coefficients. We removed outlier samples based on the sample clustering results (Fig. 4A). When $\beta = 10$ (scale-free distribution), the gene association was maximally consistent with the scale-free distribution $R2 = 0.8623843$. Consequently, we set the soft threshold of 10 to build the scale-free network Fig. 4C). Finally, seven modules were identified (Fig. 4B). The brown and lime green modules were highly correlated with the pathology grade; therefore, they were selected as clinically important modules for further analysis (Fig. 4D). The PRDEGs were utilized for intersection analysis with the brown and lime green module genes (Fig. 4E), and 15 intersecting genes were obtained. PPI network was performed through the STRING database (Fig. 4F), which yielded 13 intersecting genes with protein interactions, including *Tnf*, *Tlr2*, *Casp8*, *Icam1*, *Il1rn*, *Irf1*, *Cebpb*, *Trem1*, *Clec5a*, *Chil1*, *Osm*, *Ptx3*, and *Prtn3*. A larger line represents a greater degree of the node, and a thicker line represents a greater number of edge mediators. Subsequently, a bar graph was constructed to demonstrate the number of interactions occurring for each intersecting gene (Fig. 4G). Subnetwork construction was performed using MCODE, which clusters the network to construct functional modules (Fig. 4H), revealing dense regions of potential biological functions. *Irf1*, *Icam1*, *Tlr2*, *Tnf*, *Cebpb*, *Il1rn*, and *Casp8* were identified as hub genes.

CeRNA interaction network and correlation analysis

A ceRNA network was constructed using the starBase database for seven hub genes. The miRNAs with interworking relationships were retrieved through the seven hub genes, lncRNA-generating relationships were retrieved based on the miRNAs, and an interworking network was constructed based on the interworking relationships (Fig. 5A). Correlation analysis was subsequently demonstrated using corrplot in GSE131193 for the 35 PRDEGs obtained in GSE202659 (Fig. 5C), showing the P value and correlation coefficient of the PRDEGs, respectively.Construction of CIRI-related Molecular Subtypes.

Twelve samples from the CIRI group in GSE131193 were extracted, and the CIRI samples were classified by hierarchical clustering into two subtypes, Cluster1 and Cluster2 (Fig. 5B), and the expression of PRDEGs in the subtypes was demonstrated by a heat map. Subsequently, the expression of 35 PRDEGs between subtypes was analyzed (Fig. 5D), which demonstrated significantly different PRDEGs with $p < 0.05$, and the genes screened were *Ptx3*, *Tubb6*, *Myd88*, *Il1rn*, *Cd14*, *Icam1*, *Vim*, *Stat3*, *Epha2*, *Nfe2l2*, *Pecam1*, *Trem1*, *Tnf*, *Ripk1*, *Casp8*, *Birc3*, *Cebpb*, *Osm*, *Ezh2*, *Slc16a4*, *Apaf1*. Genes such as *Vim* in GSE131193 have a high expression profile in Cluster2, whereas the *Slc16a4* gene has the property of being highly expressed in the Cluster1 isoform.

CIRI immune infiltration analysis

We chose 12 samples of CIRI group in GSE131193 to immune cell infiltration analysis according to the CIBERSORT algorithm, (Fig. 5E). Only cells expressed in most samples, such as memory B cells, CD4 naïve T cells, Th2 cells, and M2 macrophages, were retained in the heat map. As shown, cells such as CD4 naïve T cells, monocytes, and M0 macrophages showed a high degree of infiltration in CIRI samples. Subsequently, the GSE131193 hub genes, *Irf1*, *Icam1*, *Tlr2*, *Tnf*, *Cebpb*, *Il1rn*, and *Casp8*, were extracted and correlated with 11

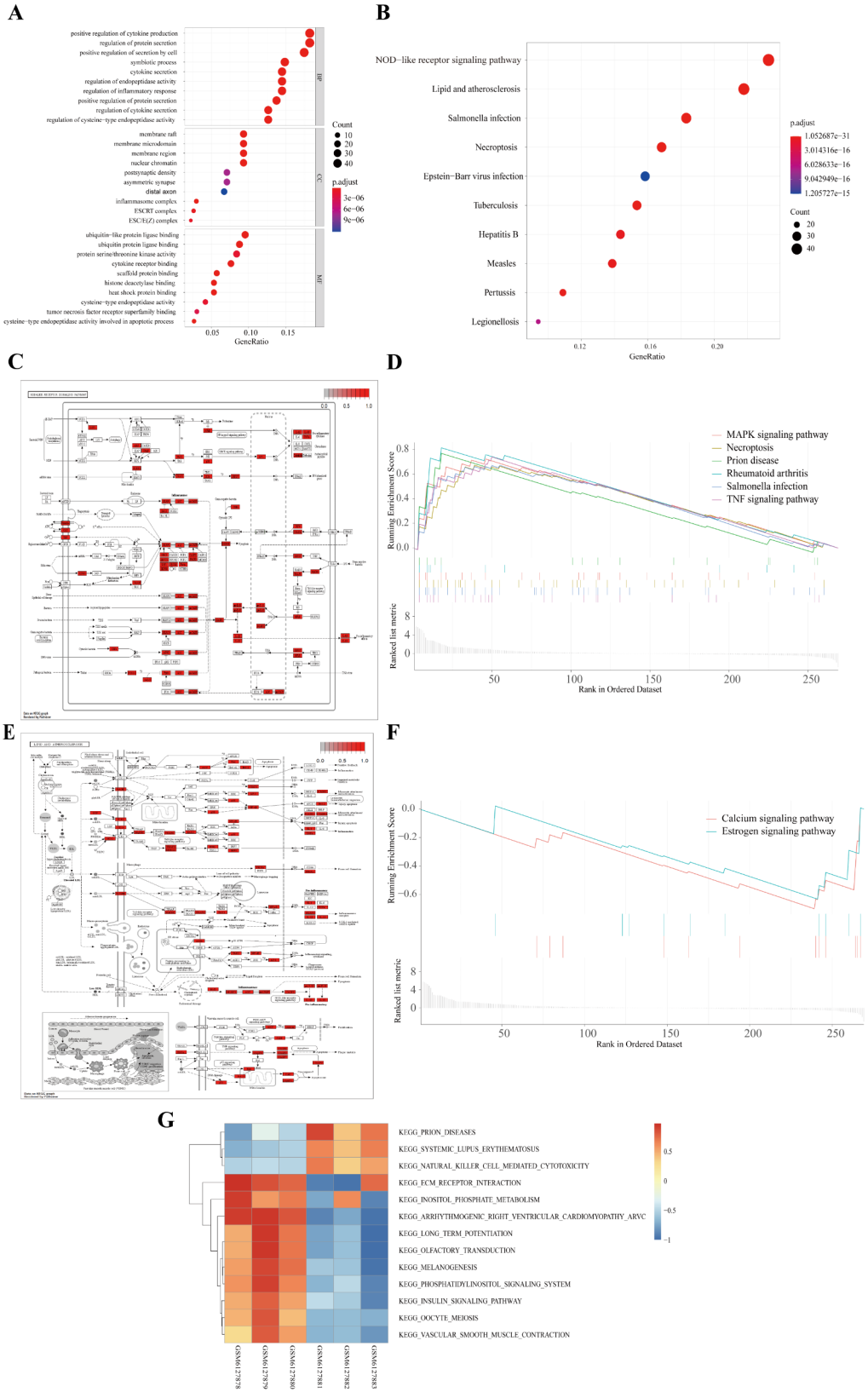

Fig. 3 Enrichment analysis of PRGs based on GSE202659. (**A**) GO. (**B**) KEGG pathway enrichment analysis. (**C**) Pathway map of the NOD-like receptor signaling pathway. (**D**) GSEA. (**E**) Pathway map of lipid and atherosclerosis. (**F**) Down-regulated pathway enrichment analysis. (**G**) GSVA

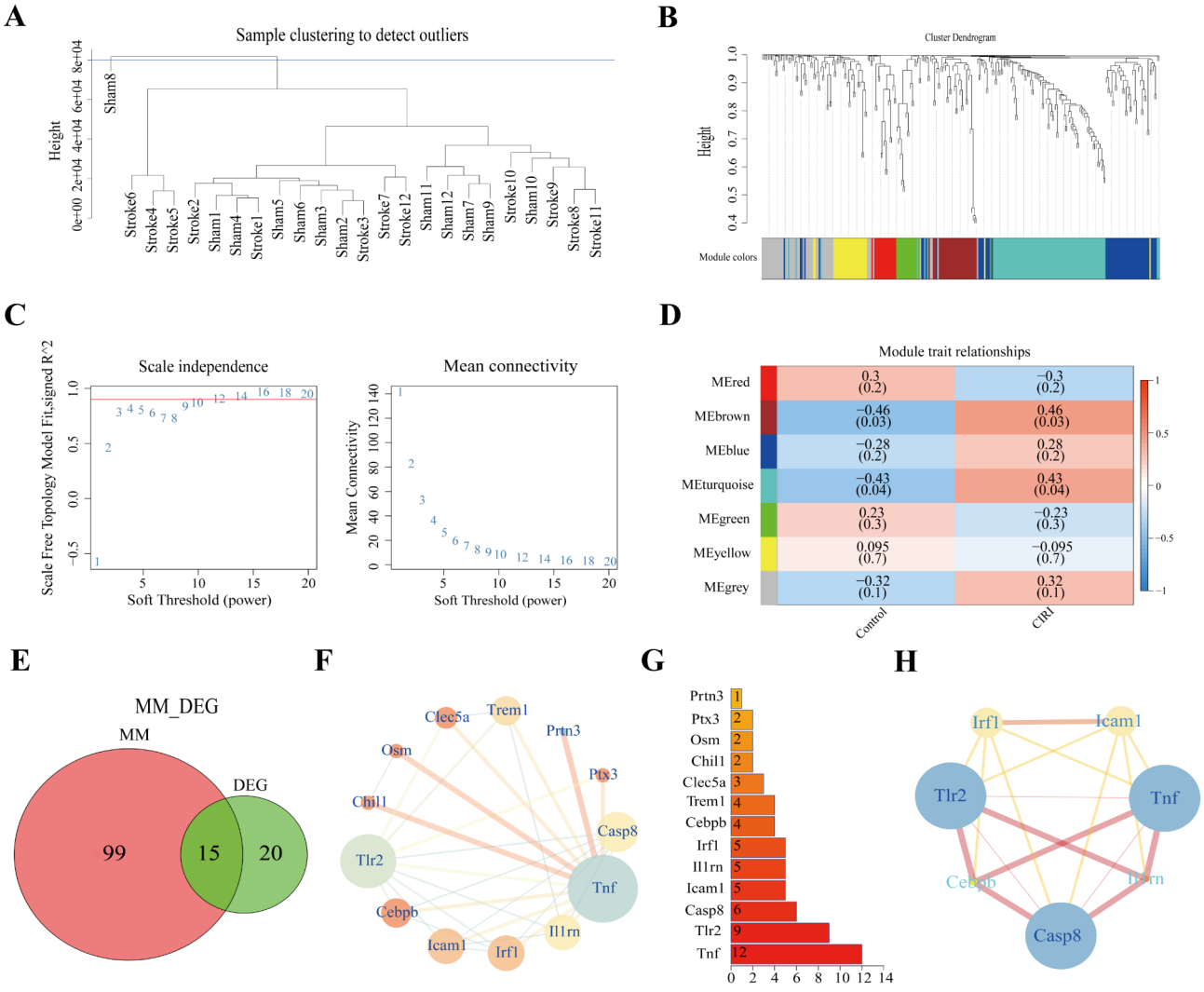

Fig. 4 CIRI gene hub gene screening. (**A**) Clustering dendrogram for 24 samples. (**B**) Dendrogram of all PRGs clustered based on the dissimilarity measure (1-TOM). (**C**) Determination of soft thresholds for WGCNA. (**D**) Heatmap of the correlation between genes characterized by the GSE131193 module and clinical features. (**E**) PRDEGs were intersected with modular genes to determine the intersecting genes. (**F**) Protein interactions. (**G**) Statistics on the number of protein interactions. (**H**) Construction of sub-networks based on the protein interactions of intersecting genes

immune cells. The results showed that *Cebpb* ($r = 0.76$), *Il1rn* ($r = 0.72$), and *Casp8* ($r = 0.69$) were positively correlated with the degree of NK cell activation. *Casp8* (r=-0.38), *Icam1* (r=-0.72), *Tlr2* (r=-0.53), *Tnf* (r=-0.46), *Cebpb* (r=-0.46), *Il1rn* (r=-0.44), *Irf1* (r=-0.57), and memory B cells were negative correlation (Fig. 5F).

The MCAO model and pyroptosis

After 24 h of ischemia/reperfusion treatment, mice in the MCAO group showed significantly higher scores for neurological deficits and weakened neurological function ($^{*}p < 0.05$, Fig. 6A), and the volume of cerebral infarcts was obviously larger than that of the sham group ($^{**}p < 0.01$, Fig. 6B-C). HE staining showed that after the induction of CIRI, neurons in the cerebral cortex were disorganized, swollen, and reduced in size. The nuclei were fixed and deeply stained. However, the nucleoli were not obvious, and the number of necrotic cells increased (Fig. 6E). Nissl staining revealed a loss of Nissl bodies in mice after MCAO (Fig. 6F).The relative mRNA expression levels of pyroptosis-related genes (*caspase-1*, *NLRP3*, *GSDMD*, *IL-1β*,*IL-18*, and *ASC*) were upregulated after MCAO ($^{*}p < 0.05$, $^{**}p < 0.01$, $^{\#}p < 0.0001$, Fig. 6D).The levels of *IL-1β* and *IL-18* in the serum were increased by ELISA compared with the Sham group ($^{***}p < 0.001$,$^{\#}p < 0.0001$, Fig. 6G, H).The protein levels of Pyroptosis-related genes (*GSDMD*, *caspase-1*, and *NLRP3*) in the MCAO group were highly increased($^{*}p < 0.05$, $^{**}p < 0.01$, $^{***}p < 0.001$, Fig. 6I, J).

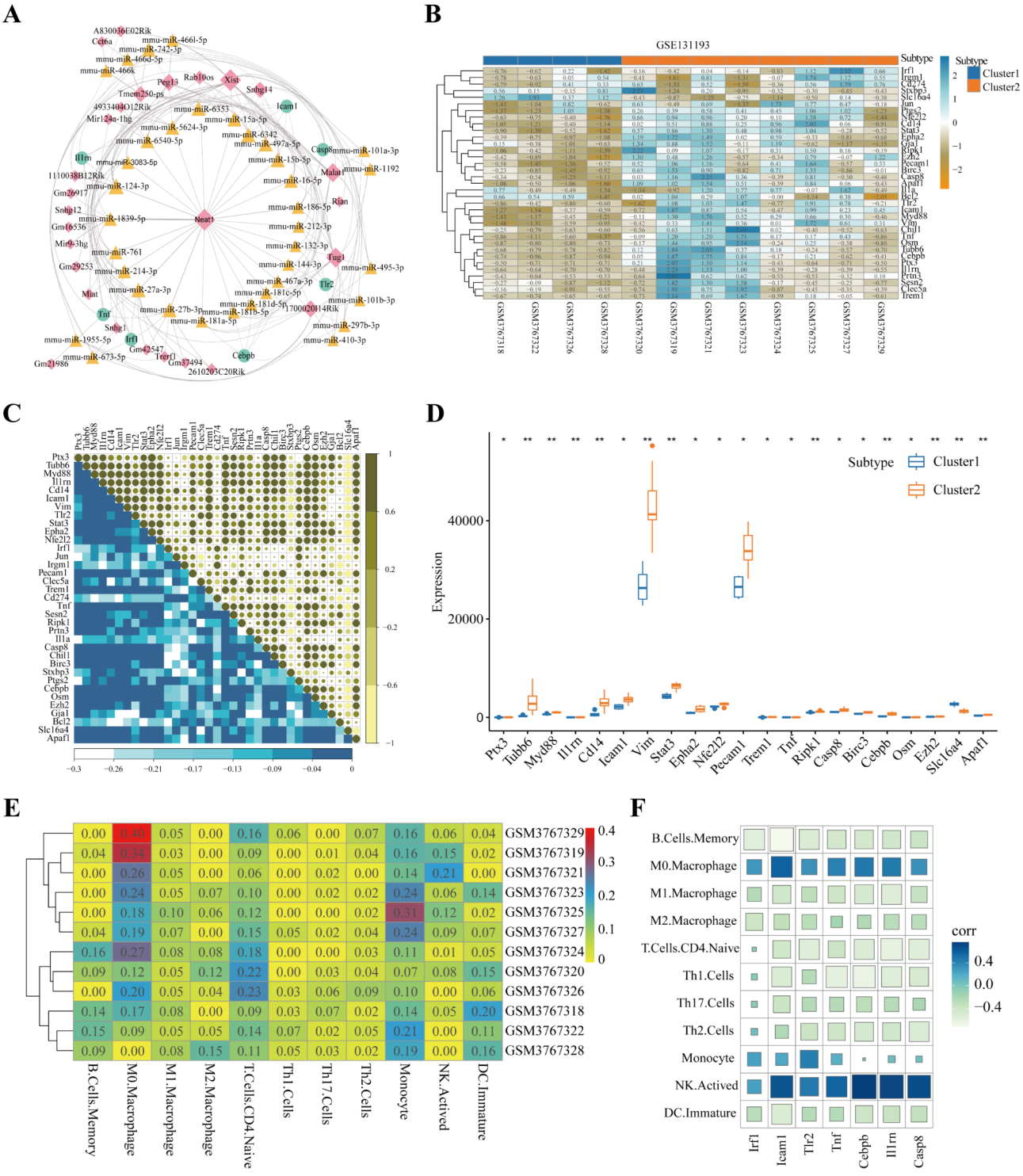

Fig. 5 Construction of a ceRNA interaction network and immune infiltration analysis of CIRI based on hub genes. (**A**) Construction of a ceRNA interaction network based on hub genes. (**B**) Heatmap of the expression of 35 PRDEGs in GSE131193 in both subtypes. (**C**) Correlation analysis of PRDEGs in GSE131193. (**D**) Heatmap of 21 significant PRDEGs in GSE131193 expressed in two isoforms. *$p < 0.05$, **$p < 0.01$. (**E**) Heatmap of 11 immune cell infiltrations in 12 CIRI samples in GSE131193. (**F**) Correlation of 11 immune cell infiltrations in GSE131193 with hub genes correlation heatmap

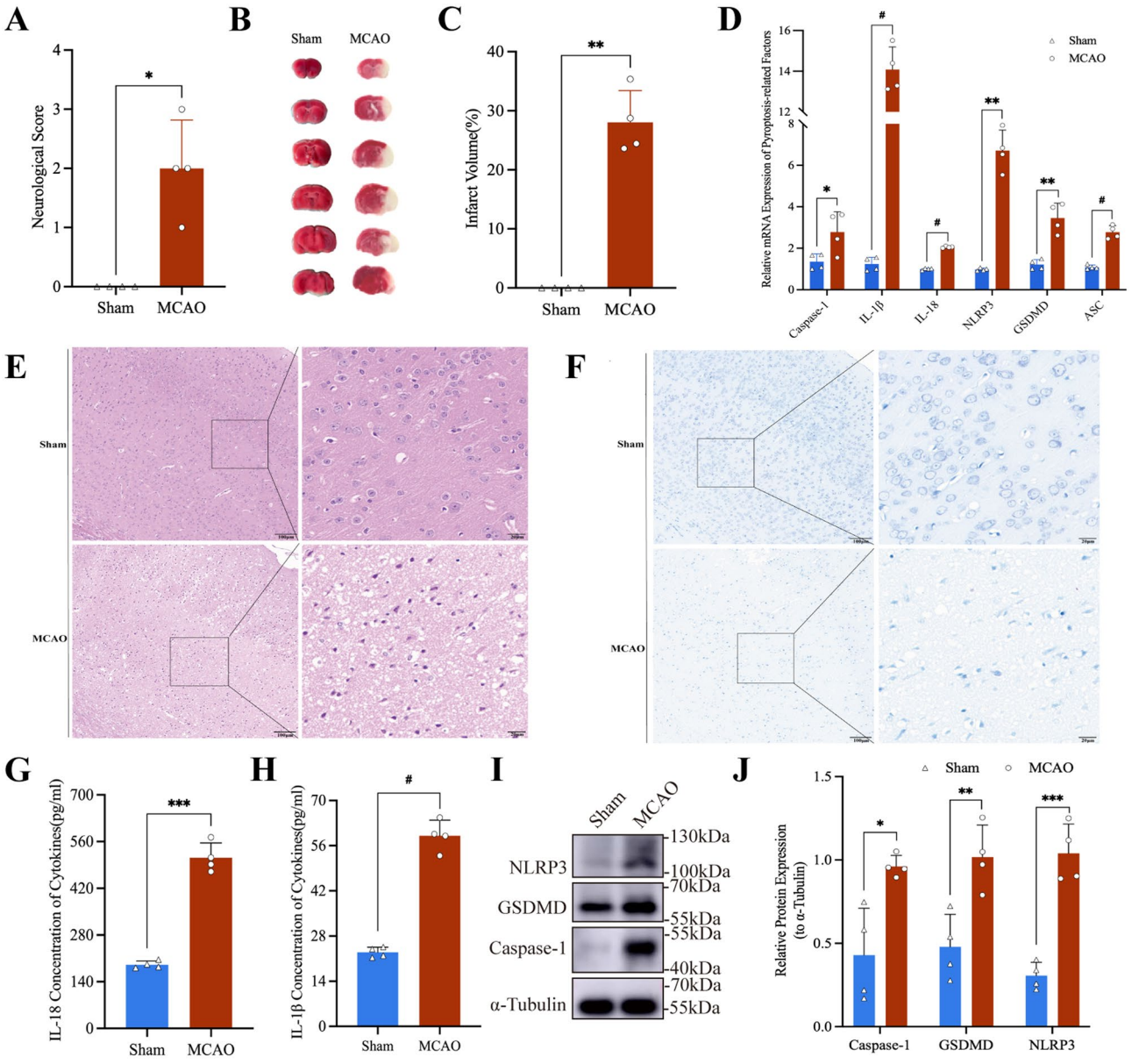

Fig. 6 Validation of the MCAO model and pyroptosis in sham and MCAO groups. (**A**) Neurobehavioral scores. (**B**) TTC staining. (**C**) Percentage of cerebral infarction. (**D**) RT-PCR of pyroptosis-related genes. (**E**) HE staining. (**F**) Nissl staining. (**G**) *IL-1β* in mouse serum. (**H**) *IL-18* in mouse serum. (**I**, **J**) Western blot of pyroptosis-related genes in sham (left) and MCAO (right) groups (to α-Tubulin). Compared with the Sham group, $^{*}p < 0.05$, $^{**}p < 0.01$, $^{***}p < 0.001$, $^{\#}p < 0.0001$, $n = 4$

RT-PCR, Western blot, and Immunofluorescence verification of hub gene expression profiles

The relative mRNA expression levels of the seven hub genes shown that compared to the sham group, *Irf1*, *Icam1*, *Tlr2*, *Cebpb*, and *Il1rn* were highly expressed in the MCAO group ($^{*}p < 0.05$, $^{\#}p < 0.0001$, *ns*, *not statistically significant*, Fig. 7A). Furthermore, immunofluorescence and western blot demonstrated an upregulation of *Irf*1 significantly in the cortical area of CIRI in mouse of the MCAO group (Fig. 7B-E).

Discussion

IS are a common acute cerebrovascular disease with high lethality and disability worldwide and is a major impediment to the recovery process of IS [26], mainly involving oxidative stress, inflammatory response, autophagy, apoptosis, and the toxic effects of excitatory amino acids. Attenuation of CIRI is key to the clinical treatment of IS. Previous studies have shown a relationship between pyroptosis and the development of IS; however, no exact target or therapeutic mechanism for pyroptosis in IS brain tissue has been identified. Pyroptosis may serve as

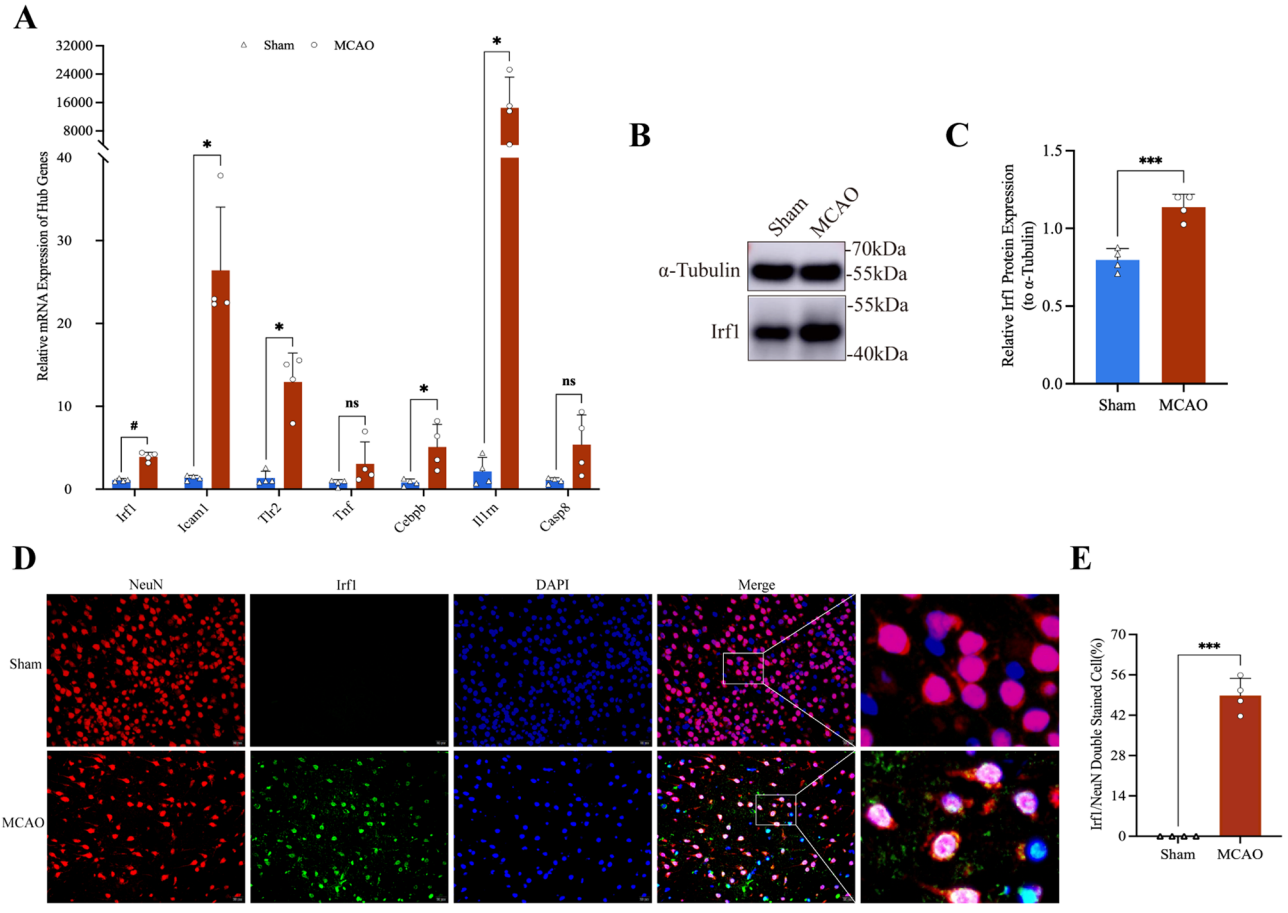

Fig. 7 Expression of Hub genes in the brain tissues of mice. (**A**) RT-PCR of hub genes in sham and MCAO groups. (**B**, **C**) Western blot of Irf1 in sham (left) and MCAO (right) groups (to α-Tubulin). (**D**) Immunofluorescence in sham and MCAO groups (Scale bar, 20 μm). (**E**) Percentage of *Irf1/NeuN* double stained cells in sham and MCAO groups. Compared with the Sham group, $^{*}p < 0.05$, $^{***}p < 0.001$, $^{\#}p < 0.0001$, *ns*, *not statistically significant*, $n = 4$

a potential target for the treatment of ischemic stroke. Therefore, mining the hub genes involved in IS pyroptosis based on bioinformatics and animal experiments is important to further explore the pathogenesis of IS from the perspective of pyroptosis.

In this study, the GO and KEGG analyses of GSE202659 and GSE131193 revealed that CIRI pyroptosis genes were mainly involved in membrane raft, positive regulation of cytokine production, ubiquitin – like protein ligase binding, Salmonella infection pathway, Lipid and atherosclerosis, and NOD – like receptor signaling pathway. And we performed GSEA and GSVA analyses on all genes, and the results were similar to the above, suggesting that pyroptosis is closely related to CIRI and that pyroptosis-associated pathways may be involved in IS. We performed WGCNA analysis based on PRGs. Subsequently, STRING and Cytoscape were applied to construct and visualize PPI network with GSE131193 and PRDEGs. Seven hub genes related to CIRI were screened, namely, *Irf1*, *Icam1*, *Tlr2*, *Tnf*, *Cebpb*, *Il1rn*, and *Casp8*. Subsequently, we conducted a series of correlation analyses. We performed immune cell infiltration analysis and found a significant positive correlation between *Cebpb*, *Il1rn*, and *Casp8*, and the degree of NK-activated infiltration while a highly significant negative correlation between *Icam1* and memory B cells. We hypothesize that the upregulation of the hub genes may play an indispensable role the development of pyroptosis in CIRI. Providing evidence to corroborate this hypothesis, our animal experiment results suggested that the mRNA levels of these five hub genes (*Irf1*, *Icam1*, *Tlr2*, *Cebpb*, and *Il1rn*), especially the most pronounced trend was in *Irf1*, were consistent with our analytical findings.

Interferon regulatory factor 1 (*Irf1*) was the first efficient regulator with the function of regulating the transcriptional expression of interferon. The encoded protein plays a role in apoptosis, cell proliferation, DNA damage response, and immune response. This suggests a potential role for *IRF1* in inflammation and immunity.*IRF1* deficiency leads to mucosal inflammation and reduced mucosal bacterial levels in TNFα-primed colon [27]. It has been found that in the natural immune response [28, 29], activation of the pyroptosis pathway activates GSDMD of the gasdermin family, which mediates

pyroptosis to antagonize and clear pathogenic bacterial infections. Additionally, Fan et al. [30] found the nonclassical NF-κB pathway makes the development of atherosclerotic heart disease in an IRF-1-dependent manner through activation of GSDMD, which promotes endothelial pyroptosis. And clinically, IRF-1 immunoreactivity in inflammatory cells and brain neurons in IS patients who died 1–2 days [31]. A recent study has found that *Irf1* is upregulated in transcranial magnetic stimulation effect of IS via bioinformatics analysis [32], which is consistent with our previous findings. In general, these findings indicated *Irf1* may be a significant involvement in CIRI and pyroptosis, but the function of *Irf1* is currently unknown.

CCAAT enhancer binding protein beta (*Cebpb*) is involved in apoptosis, immune regulation, inflammatory response, and energy metabolism of tumor cells through the recognition and binding of the regulatory regions of target genes. Kim Newton [33] found that *Cebpb* regulates the expression of pro-inflammatory genes by targeting the enhancer region, which in turn affects the activation state of microglia, and accelerate neurodegenerative lesions. Meanwhile, Li [34]found that *Cebpb* is upregulated in MCAO, which is in agreement with the results of our study, and microRNA-381-3p confers protection against IS by suppressing *Cebpb*. Subsequent research [35] has found that down-regulation of *Cebpb* in in vivo and in vitro studies suppressed pyroptosis-associated activation of NLRP3 inflammatory vesicles and ameliorated lupus nephritis-associated impairment of renal structure and function. Therefore, the influence of *Cebpb* on the progression of neurological diseases may be linked to its role in activating pyroptosis and immune pathways, and there is limited literature. In addition, one study [36] has found that in prostate cancer patients and mouse models, c/ebpβ is a key transcription factor, whose activation can cause NK cell mitochondrial dysfunction and increase the accumulation of reactive oxygen species, thereby affecting its anti-tumor effector function, which also supports our findings. But the function of *Cebpb* in CIRI NK-activated infiltration is still presently unknown.

Interleukin 1 Receptor Antagonist (*Il1rn*), also known as IL-1RA, competitively binds to the IL-1β receptor to exert an anti-inflammatory effect and regulate immune status. Zheng et al. [37] found that raleukin, a recombinant IL-1RA, effectively prevented medication-related osteonecrosis of the jaw in vivo through alleviating NLRP3 inflammasome activation and pyroptosis. A clinical study [38] found elevated *Il1rn* expression in the plasma of patients after stroke. And the results of our animal experiments also showed that *Il1rn* expression was upregulated after CIRI, but the mechanism of *Il1rn*'s role in relation to IS pyroptosis and immunity has not yet been clarified.

Intercellular Cell Adhesion Molecule-1 (*Icam1*) plays important roles in mediating cell-cell adhesion, which would shift from a lower level in the resting state to a higher expression level when stimulated by a variety of inflammatory factors, and is mainly involved in leukocyte transport and immune cell recruitment [39]. For example, ICAM1 expression was upregulated in damaged cerebrovascular endothelial cells after stroke, and neutrophils interacted with integrin Mβ2 and ICAM1 across the BBB to further cause brain injury [40]. Therefore, we can seek to develop new stroke drugs from the perspective of *Icam1*. Luo [41] has found that anti-β2-glycoprotein I (an anti-phospholipid antibody) can be observed to induce neutrophil pyroptosis, which enhanced the expression of ICAM-1 and IL-8 in endothelial cells in cerebral infarction. The trend of *Icam1* above literatures was respectively consistent with our previous results. However, the molecular mechanism of ICAM-1 in CIRI and pyroptosis has not been clarified. Liu found that moderate-to-severe SLE patients with high ICAM-1 expression mediated less B cell activation and IgG production [42]. Our results also showed that there is a highly significant negative correlation between *Icam1* and memory B cells, but and more functional studies are required to confirm.

Toll Like Receptor 2 (*Tlr2*) is a member of the Toll like receptor family, which recognizes damage associated molecular patterns (DAMPs) and triggers immune responses [43]. *Tlr2* plays a key role in the pathological process of IS, and its expression is upregulated after stroke, which in turn triggers an inflammatory response and exacerbates brain damage [44]. The trend of *Tlr2* was consistent with our findings. Many studies have shown that neuroprotection is achieved in CIRI by inhibiting the TLR2/NF-κB-mediated inflammatory pathway. For example, cyclovibuxine D(CVB-D) is widely used to treat cardiovascular diseases in the clinical. Iu et al. [45] found that CVB-D could inhibit neuroinflammatory responses and reduce oxidative stress by inhibiting the TLR2/4-NF-κB signaling pathway on permanent IS in rats. At the same time, it has been found [46] that glycolysis inhibitors can inhibit pyroptosis and oxidative stress by down-regulating TLR2 expression, which in turn ameliorates allergic airway inflammation. It follows that *Tlr2* may play a role in CIRI through the pyroptosis pathway, which is still presently unknown, and therefore more experiments are needed to study it.

Although this study identified key genes (*Irf1*, *Icam1*, *Tlr2*, *Cebpb*, and *Il1rn*) that are closely associated with pyroptosis and CIRI, and verified upregulation of gene expression in MCAO, there are some limitations to this study. The scope of analysis in this study focused on the gene level and has not yet explored protein expression in depth. Future research will further validate the function of these genes through experiments in vivo and vitro

such as western blot and immunofluorescence staining. In addition, as only a mouse model was used, the applicability of the conclusion to human stroke still needs to be verified by more clinical samples. And we plan to increase the sample size to dig deeper into the biological mechanisms so as to further validate the findings of this study.

Conclusions

In summary, a comprehensive analysis of bioinformatics and animal experiments revealed that the *Irf1*, *Icam1*, *Tlr2*, *Cebpb*, and *Il1rn* genes are the hub genes for pyroptosis in CIRI. The immune infiltration analysis was also investigated. This provides a new idea for future research on the prevention and treatment of IS from the perspective of pyroptosis, and none of which have been sufficient research on CIRI. But our research still requires additional basic experimental and clinical validation to confirm its results.

Abbreviations

CIRI	cerebral ischemia/reperfusion injury
PRGs	cerebral ischemia/reperfusion injury
PRDEGs	pyroptosis-related differentially expressed genes
GO	gene ontology
GEO	gene expression omnibus
KEGG	kyoto encyclopedia of gene genomes
GSEA	gene set enrichment analysis
GSVA	gene set variation analysis
PPI	protein-protein interaction
MCAO	middle cerebral artery occlusion
IS	ischemic stroke
ceRNA	competing endogenous RNA
ELISA	enzyme linked immunosorbent assay
RT-PCR	reverse transcription-polymerase chain reaction
WGCNA	weighted correlation network analysis
CIBERSORT	cell type identification by estimating relative subsets of RNA transcripts

Supplementary Information

The online version contains supplementary material available at https://doi.org/10.1186/s12920-025-02119-2.

Supplementary Material 1

Supplementary Material 2

Supplementary Material 3

Supplementary Material 4

Supplementary Material 5

Acknowledgements

We acknowledge the GEO (https://www.ncbi.nlm.nih.gov/geo/) and GeneCards (https://www.genecards.org/) database for uploading meaningful datasets.

Author contributions

WZ designed the experiments and conducted the study. XYS and RW wrote the manuscript. WZ revised the manuscript. XYS and RW conducted the design and operation of experimental animals. DY contributed to literature search and data collection. Most of the analyses were performed by XYS, RW, and BWY. WZ provided financial support. All authors have read and approved of the contents of the manuscript prior to submission.

Funding

This study was supported by National Natural Science Foundation of China (Grant 82160374, and 82360370), and applied basic research foundation of Yunnan Province (Grant 202101AY070001-021).

Data availability

The datasets supporting the conclusions of this article are included within the article and its Additional files.

Declarations

Ethics approval and consent to participate

The study for mice is compliant with all relevant ethical regulations for animal experiments. All experiments and facilities were approved by the Laboratory Animal Ethics Review Committee of Kunming Medical University (License No. kmmu20221789) and were conducted in conformity to the Guidelines for Animal Experiments, the Laboratory Animal Center of Kunming Medical University.

Consent for publication

Not applicable.

Competing interests

The authors declare no competing interests.

Author details

[1]Department of Emergency Medicine, The First Affiliated Hospital of Kunming Medical University, No. 295 Xichang Road, Wu Hua District, Kunming, Yunnan Province 650032, China

Received: 9 December 2024 / Accepted: 28 February 2025
Published online: 16 March 2025

References

1. Global regional. National burden of stroke and its risk factors, 1990–2019: a systematic analysis for the global burden of disease study 2019. Lancet Neurol. 2021;20(10):795–820.
2. Toyoda K, Yoshimura S, Nakai M, Koga M, Sasahara Y, Sonoda K, Kamiyama K, Yazawa Y, Kawada S, Sasaki M, Terasaki T, Miwa K, Koge J, Ishigami A, Wada S, Iwanaga Y, Miyamoto Y, Minematsu K. Kobayashi,Twenty-Year change in severity and outcome of ischemic and hemorrhagic strokes. JAMA Neurol. 2022;79(1):61–9.
3. Ganesh A. Goyal,Thrombectomy for acute ischemic stroke: recent insights and future directions. Curr Neurol Neurosci Rep. 2018;18(9):59.
4. Turc G, Tsivgoulis G, Audebert HJ, Boogaarts H, Bhogal P, De Marchis GM, Fonseca AC, Khatri P, Mazighi M, de la Ossa NPérez, Schellinger PD, Strbian D, Toni D, White P, Whiteley W, Zini A, van Zwam W, Fiehler J. European stroke organisation (ESO)-European society for minimally invasive neurological therapy (ESMINT) expedited recommendation on indication for intravenous thrombolysis before mechanical thrombectomy in patients with acute ischemic stroke and anterior circulation large vessel occlusion,J Neurointerv Surg,14(3)(2022):209.
5. Cookson BT. Brennan,Pro-inflammatory programmed cell death. Trends Microbiol. 2001;9(3):113–4.
6. Shi J, Gao W, Shao F. Pyroptosis: Gasdermin-Mediated programmed necrotic cell death. Trends Biochem Sci. 2017;42(4):245–54.
7. Moujalled D, Strasser A, Liddell JR. Molecular mechanisms of cell death in neurological diseases. Cell Death Differ. 2021;28(7):2029–44.
8. Li W, Shen N, Kong L, Huang H, Wang X, Zhang Y, Wang G, Xu P. Hu,STING mediates microglial pyroptosis via interaction with NLRP3 in cerebral ischaemic stroke. Stroke Vasc Neurol. 2024;9(2):153–64.
9. Li J, Hao JH, Yao D, Li R, Li XF, Yu ZY, Luo X, Liu XH, Wang MH, Wang W. Caspase-1 Inhibition prevents neuronal death by targeting the canonical inflammasome pathway of pyroptosis in a murine model of cerebral ischemia. CNS Neurosci Ther. 2020;26(9):925–39.

10. Global regional. National burden of stroke and its risk factors, 1990–2021: a systematic analysis for the global burden of disease study 2021. Lancet Neurol. 2024;23(10):973–1003.
11. Liu Y, Wang W, Cui X, Lyu J, Xie Y. Exploring genetic associations of 3 types of risk factors with ischemic stroke: an integrated bioinformatics study. Stroke. 2024;55(6):1619–28.
12. Davis S S, Meltzer P P. GEOquery: a Bridge between the gene expression omnibus (GEO) and bioconductor. Bioinformatics. 2007;23(14):1846–7.
13. Barrett T, Wilhite S.E., Ledoux P, Evangelista C, Kim I.F., Tomashevsky M, Marshall K.A., Phillippy K.H., Sherman P.M., Holko M, Yefanov A, Lee H, Zhang N, Robertson C.L., Serova N, Davis S, Soboleva A. NCBI GEO: archive for functional genomics data sets–update. Nucleic Acids Res. 2013;41(Database issue):D991–995.
14. Kestner RI, Mayser F, Vutukuri R, Hansen L, Günther S, Brunkhorst R, Devraj K. W. Pfeilschifter,Gene expression dynamics at the neurovascular unit during early regeneration after cerebral ischemia/reperfusion injury in mice,front neurosci,14(2020):280.
15. Liu J, Guo X, Yang L, Tao T, Cao J, Hong Z, Zeng F, Lu Y, Lin C. Qin,Effect of Celastrol on LncRNAs and mRNAs profiles of cerebral Ischemia-Reperfusion injury in transient middle cerebral artery occlusion mice model. Front Neurosci. 2022;16:889292.
16. Androvic P, Kirdajova D, Tureckova J, Zucha D, Rohlova E, Abaffy P, Kriska J, Valny M, Anderova M, Kubista M. Valihrach,Decoding the transcriptional response to ischemic stroke in young and aged mouse brain. Cell Rep. 2020;31(11):107777.
17. Stelzer G, Rosen N, Plaschkes I, Zimmerman S, Twik M, Fishilevich S, Stein TI, Nudel R, Lieder I, Mazor Y, Kaplan S, Dahary D, Warshawsky D, Guan-Golan Y, Kohn A, Rappaport N, Safran M. D. Lancet,The GeneCards Suite: From Gene Data Mining to Disease Genome Sequence Analyses,Curr Protoc Bioinformatics,54(2016):1.30.31–31.30.33.
18. Ritchie ME, Phipson B, Wu D, Hu Y, Law CW, Shi W. Smyth,limma powers differential expression analyses for RNA-sequencing and microarray studies. Nucleic Acids Res. 2015;43(7):e47.
19. Shannon P., Markiel A., Ozier O., Baliga N.S., Wang J.T., Ramage D., Amin N., Schwikowski B., Ideker T. Cytoscape: a software environment for integrated models of biomolecular interaction networks. Genome Res. 2003;13(11):2498–504.
20. Assenov Y, Ramírez F, Schelhorn SE, Lengauer T, Albrecht M. Computing topological parameters of biological networks. Bioinformatics. 2008;24(2):282–4.
21. Bader GD. Hogue,An automated method for finding molecular complexes in large protein interaction networks. BMC Bioinformatics. 2003;4:2.
22. Li JH, Liu S, Zhou H, Qu LH, Yang JH. StarBase v2.0: decoding miRNA-ceRNA, miRNA-ncRNA and protein-RNA interaction networks from large-scale CLIP-Seq data. Nucleic Acids Res. 2014;42(Database issue):D92–97.
23. Chen Z, Huang A, Sun J, Jiang T, Qin FX. Wu Inference Immune Cell Composition Expression Profiles Mouse Tissue Sci Rep. 2017;7:40508.
24. Zhu L, Dai S, Lu D, Xu P, Chen L, Han Y, Zhong L, Chang L. Wu,Role of NDEL1 and VEGF/VEGFR-2 in mouse Hippocampus after status epilepticus. ASN Neuro. 2020;12:1759091420926836.
25. Bederson JB, Pitts LH, Tsuji M, Nishimura MC, Davis RL, Bartkowski H. Rat middle cerebral artery occlusion: evaluation of the model and development of a neurologic examination. Stroke. 1986;17(3):472–6.
26. Strubakos CD, Malik M, Wider JM, Lee I, Reynolds CA, Mitsias P, Przyklenk K, Hüttemann M. Sanderson,Non-invasive treatment with near-infrared light: A novel mechanisms-based strategy that evokes sustained reduction in brain injury after stroke. J Cereb Blood Flow Metab. 2020;40(4):833–44.
27. Tan G, Huang C, Chen J, Chen B, Shi Y, Zhi F. An IRF1-dependent pathway of TNFα-induced shedding in intestinal epithelial cells. J Crohns Colitis. 2022;16(1):133–42.
28. Liu X, Zhang Z, Ruan J, Pan Y, Magupalli VG, Wu H. J. Lieberman,Inflammasome-activated gasdermin D causes pyroptosis by forming membrane pores,Nature,535(7610)(2016):153–8.
29. Wang K, Sun Q, Zhong X, Zeng M, Zeng H, Shi X, Li Z, Wang Y, Zhao Q, Shao F. J. Ding,Structural mechanism for GSDMD targeting by autoprocessed caspases in Pyroptosis,Cell,180(5)(2020):941–e955920.
30. Fan X, Li Q, Wang Y, Zhang DM, Zhou J, Chen Q, Sheng L, Passerini AG. Sun,Non-canonical NF-κB contributes to endothelial pyroptosis and atherogenesis dependent on IRF-1. Transl Res. 2023;255:1–13.
31. Alexander M, Forster C, Sugimoto K, Clark HB, Vogel S, Ross ME, Iadecola C. Interferon regulatory factor-1 immunoreactivity in neurons and inflammatory cells following ischemic stroke in rodents and humans. Acta Neuropathol. 2003;105(5):420–4.
32. Zhao M, Liu A, Wu J, Mo L, Lu F. Wan,Il1r2 and Tnfrsf12a in transcranial magnetic stimulation effect of. Ischemic Stroke Via Bioinf Anal Med (Baltimore). 2024;103(4):e36109.
33. Ndoja A, Reja R, Lee SH, Webster JD, Ngu H, Rose CM, Kirkpatrick DS, Modrusan Z, Chen YJ, Dugger DL, Gandham V, Xie L, Newton K. V.M. Dixit,Ubiquitin ligase COP1 suppresses neuroinflammation by degrading C/EBPβ in Microglia,Cell,182(5)(2020):1156–e11691112.
34. Li J, Lv H, Che Y. microRNA-381-3p confers protection against ischemic stroke through promoting angiogenesis and inhibiting inflammation by suppressing Cebpb and Map3k8. Cell Mol Neurobiol. 2020;40(8):1307–19.
35. Wang X, Cheng W, Chen X, Gong Y, Wang G, Zhang X. Y. Qi,Inhibition of CEBPB attenuates lupus nephritis via regulating Pim-1 signaling,mediators Inflamm,2022(2022):2298865.
36. Portale F., Carriero R, Iovino M, Kunderfranco P, Pandini M, Marelli G, Morina N, Lazzeri M, Casale P, Colombo P, De Simone G, Camisaschi C, Lugli E, Basso G, Cibella J, Marchini S, Bordi M, Meregalli G, Garbin A, Dambra M, Magrini E, Rackwitz W, Cecconi F, Corbelli A, Fiordaliso F, Eitler J, Tonn T, Di Mitri D. C/EBPβ-dependent autophagy Inhibition hinders NK cell function in cancer. Nat Commun. 2024;15(1):10343.
37. Zheng Y, Wang X, He Y, Chen S, He L, Zhang Y. Exosomes from Adipose-Derived mesenchymal stromal cells prevent Medication-Related osteonecrosis of the jaw by inhibiting macrophage M1 polarization and pyroptosis. Int J Nanomed. 2024;19:12675–93.
38. Becker K.J., Dankwa D., Lee R., Schulze J., Zierath D., Tanzi P., Cain K., Dressel A., Shibata D., Weinstein J., Stroke. IL-1ra, IL1RN, infection and outcome. Neurocrit Care. 2014;21(1):140–6.
39. Liu S, Zhang Z, He Y, Kong L, Jin Q, Qi X, Qi D. Gao,Inhibiting leukocyte-endothelial cell interactions by Chinese medicine Tongxinluo capsule alleviates no-reflow after arterial recanalization in ischemic stroke. CNS Neurosci Ther. 2023;29(10):3014–30.
40. Pan J, Wang Z, Huang X, Xue J, Zhang S, Guo X. Zhou,Bacteria-Derived Outer-Membrane vesicles hitchhike neutrophils to enhance ischemic stroke therapy. Adv Mater. 2023;35(38):e2301779.
41. Luo J, Zhang M, Wang Z, Yan L, Liu Y. Anti–β(2)GPI/β(2)GPI induces neutrophil pyroptosis and thereby enhances ICAM–1 and IL–8 expression in endothelial cells. Int J Mol Med,49(5)(2022).
42. Liu S, Liu ZC, Zhang MY, Wang SJ, Pan M, Ji P, Zhu C, Lin P. Y. Wang,ICAM-1 mediated cell-cell adhesion exerts dual roles on human B cell differentiation and IgG production,iScience,26(12)(2023):108505.
43. Sims GP, Rowe DC, Rietdijk ST, Herbst R. Coyle,HMGB1 and RAGE in inflammation and cancer. Annu Rev Immunol. 2010;28:367–88.
44. Brea D, Blanco M, Ramos-Cabrer P, Moldes O, Arias S, Pérez-Mato M, Leira R, Sobrino T. Castillo,Toll-like receptors 2 and 4 in ischemic stroke: outcome and therapeutic values,j. Cereb Blood Flow Metab. 2011;31(6):1424–31.
45. Qiu Y, Yin Q, Fei Y, Li Y, Huang H, Fang W, Shen W, Liang B, Zhu X, Li Y. JLX001 modulated the inflammatory reaction and oxidative stress in pMCAO rats via inhibiting the TLR2/4-NF-κB. Signal Pathw Neurochem Res,44(8)(2019):1924–38.
46. Sha JF, Xie QM, Chen N, Song SM, Ruan Y, Zhao CC, Liu Q, Shi RH, Jiang XQ, Fei GH. Wu,TLR2-hif1α-mediated Glycolysis contributes to pyroptosis and oxidative stress in allergic airway inflammation,free. Radic Biol Med. 2023;200:102–16.

Publisher's note